SEMARAK ILMU PUBLISHING

CFD Letters

Journal homepage:
https://semarakilmu.com.my/journals/index.php/CFD_Letters/index
ISSN: 2180-1363

Exergy Efficiency and Energy Efficiency of Double Air Pass Solar Tunnel Air Dryer: A CFD Analysis

Dagim Kebede Gari[1,*], Venkata Ramayya Ancha[1], Lingala Syam Sundar[2]

[1] Department of Mechanical Engineering, Jimma Institute of Technology, Jimma University, Jimma, Ethiopia
[2] Department of Mechanical Engineering, College of Engineering, Prince Mohammad Bin Fahd University, Al-Khobar, 31952, Saudi Arabia

ARTICLE INFO

Article history:
Received 6 February 2024
Received in revised form 17 April 2024
Accepted 14 June 2024
Available online 31 October 2024

Keywords:
Energy; Exergy; Solar tunnel dryer; Numerical study; Enhancement

ABSTRACT

This work presents, the computational fluid dynamics simulation of a forced convection double air pass solar tunnel drying system to study the temperature distribution, the flow behaviour of the air stream, and the exergy performance. Realizable k-epsilon non-equilibrium wall function turbulence model, discrete ordinate radiation model, and species transport were used. The average temperature, thermal efficiency, and exergy efficiency were found to 59.2 ºC, 30%, and 9.41%, respectively. The result revealed that the uniform temperature and velocity distribution throughout the heating and drying chamber. Therefore, the newly developed double air pass solar tunnel dryer enhances the air temperature and the exergy performance leads to the increment of drying rate and reduction of drying period.

1. Introduction

Drying is a process of moisture removal from the surface of a product based on mass transfer and heat transfer phenomenon. Solar drying technique has been used to dry plants, seeds, fruits, meats, fish, and forest products, since the early stage of mankind, to benefit from the free and renewable energy source provided by the sun. However, a little research has been done on the design of appropriate solar drying systems for biomass briquettes. The biomass briquette drying is an energy intensive process that requires 70% of the total energy used in the biomass densification process [1,2]. The majority of sub Saharan African countries use open sun drying technique. Drying under open sun is not efficient and effective regarding evaporation rate, drying period, and product quality. Recently, different solar dryers were developed and proven the enhance temperature at lower relative humidity increase the drying rate, and improve the quality feature of the product compared to open sun drying.

Currently, different types of solar dryers have been developed and used to dry agricultural and industrial products to optimize the quality and improve their life [3]. Solar dryers can be classified based on different criteria, the first one is based on the mode of air circulation, i.e. forced and natural

* *Corresponding author.*
E-mail address: kdagim82@gmail.com (Dagim Kebede Gari)

https://doi.org/10.37934/cfdl.17.4.5065

convection solar dryers, the second one based on the mode of solar radiation capturing, i.e. indirect, direct, and mixed solar dryers, and the third one based on the modes of operational principle, i.e. solar cabinet dryer, and solar tunnel greenhouse dryer [4-6]. Solar cabinet dryers have been used to dry the agricultural products. However, solar tunnel greenhouse drying systems have recently received remarkable consideration among the community of researchers and engineers for the large-scale application of agricultural and industrial products [7, 8]. The technology of solar tunnel drying techniques has advanced from a simple passive-direct mode dryer to complex active-mixed mode (hybrid) dryers.

Different methodologies, modes of operation, and innovation were developed for the enhancement of thermal and drying efficiency, significant increment of drying rate to minimize drying period, for the improvement of product quality, and also to get economically feasible drying technique. Also, the drying rate can be affected by initial moisture content, water activity, drying air temperature, air velocity, relative humidity, microstructure, bulk density and porosity, chemical pretreatment, corporation ratio, and vapor pressure [9-13]. Among these factors, the drying rate is highly influenced by air temperature and velocity [14]. These factors can be mitigated by improving the geometry configuration and operating principle to achieve uniform temperature and air flow distribution [15]. Experimental and numerical investigation were employed to study the effect of temperature and air velocity behavior on the performance of solar drying system [16, 17].

Al Smin *et al.,* [18] used particle swam optimization for the experimental data of Concentrated Solar Power-Photovoltaic (CSP-PV) hybrid systems and they observe experimental results improved the effectiveness. Abdul Karim and Mohammad [19] used the sensitivity and uncertainty analyses for solar renewable energy applications. Sulaiman *et al.,* [20] conducted a review for the utilization of solar energy for the evacuated tube solar air collectors. Shameli *et al.,* [21] conducted review related to the Gold nanoparticles based nanofluids in a hybrid photovoltaic-system. Nazer *et al.,* [22] used transient thermal analysis and thermoelectric simulation of the system was through the CFD software for the experimental data of photovoltaic thermal (PVT) systems-thermoelectric generator (TEG) and found that, the error recorded between the experimental and simulation results was 4.2%. Zulakmal *et al.,* [23] used Computational Fluid Dynamics (CFD) simulation using COMSOL software for the experimental data of solar photovoltaic-thermal (PV/T)-thermoelectric generator hybrid system and observed experimental data is well agreed with the CFD data. Ab Rashid *et al.,* [24] used CFD analysis for the Homogeneous charge compression ignition (HCCI) engine and observed swirl induce piston bowl design indicate an enhancement of in-cylinder pressure for the Spiral Crown geometry model, reaching 9.42 MPa.

Yanagita *et al.,* [25] considered CFD analysis for the nasal cavity and found the ratio of the concentration to the initial concentration in Ethmoid Sinus is approximately 0.6. Jahan *et al.,* [26] used the MAPLE software to study the solar radiation and dissipative transport of steady mixed convective hybrid nanofluid flow regime for an incompressible fluid and found the rate of heat transfer is higher in all cases but the reduction of mass transfer is also noticed. Omer and Kamar [27] studied numerically about the efficiency of flat-plate solar collector (FPSC) using multi-walled carbon nanotubes (MWCNTs)/water nanofluids and found thermal efficiency increase of 6.080% and 6.857% at volume flow rate of 0.2 kg/min to 0.8 kg/min. Khairi *et al.,* [28] analyzed the centre-offset annular rotary drum using open foam and the meshing software GMSH and they used arbitrary mesh interface. They observed the quality of mesh and secures a reliable and reproducible dynamic mesh motion for the implementation of the drying process. Ismail *et al.,* [29] used Computational Fluid Dynamics (CFD) for the NACA 0012 airfoil using Laplace equation and they observed execution time for the NACA 0012 validation case yielded a parallelization efficiency above 50%. Akter *et al.,* [30] used Photovoltaic (PV) modules for the electricity production of isolated islands in the northern Bay

of Bengal and found that 10 kW microgrid SPV system can reduce CO_2 emissions by 284 tons and the payback period of the investment is 8.8 years. Koli *et al.,* [31] observed the drying time for green chilli and okra is 9 h and 5 h less in WSAH than WOSAH while OSD takes 17 h and 11 h more than WSAH and also observed the thermal efficiency is 6%, and exergy efficiency 13% lower than WSAH.

The most widely used method to study the temperature and velocity distribution throughout the drying system are computational fluid dynamics (CFD) simulation to improve the performance. Numerical techniques are more complex and time taking contain multipart mathematical equations [17]. Also, experimental investigation of temperature and air distribution under large scale solar dryer requires numerous instruments and sensors to be mounted at different location which makes the study difficult and expensive. This phenomenon enhanced the acceptance of computational fluid dynamics (CFD) software for the prediction of temperature profile, flow behavior, and for the demonstration of heat and mass transfer happening in multinary mixtures (porous media).

Different research has been done to study the temperature and velocity profile of single air pass solar tunnel dryer to improve its performance. However, there are few studies on the analysis of a double air pass solar tunnel dryer temperature and air distribution through CFD simulation. Accordingly, this study intended to analyze the temperature distribution and air flow profile of newly designed a double air pass solar tunnel drying system to improve the thermal and exergy performance through CFD simulation.

2. Geometry Creation and Mesh Generation

The geometry of a double air pass solar tunnel air dryer (DAPSTD) was developed using Solid-works software and imported to ANSYS-Fluent for CFD simulation. After the creation of geometry, the solid and fluid domains were differentiated under design modeler module. The drying system has two main chambers, a semi-cylindrical heating chamber with the diameter of 1.2 m and a rectangular shape drying chamber of 2.4 m long, 1.2 m wide and 0.6 m high. The major components and chambers of the drying system were presented in Figure 1(a).

The irregular shape of the developed geometry can be converted into more recognizable elements or volumes using meshing techniques to improve the simulation quality. The computational domain of the drying system was discretized by mesh generation as shown in Figure 1(b). The linear Hex Dominant meshing method were selected and the element types are set to all Quad to enhance the accuracy of the final result. After editing and refining mesh of the drying system, the size of the element is 0.06m, the number of elements is 88,878 and the number of nodes is 27,785 with the maximum skewness of 0.9976. Finally, the heat transfer surface boundaries were defined which are inlet, outlet, 4 absorber plate walls, 3 collector cover walls, and 5 floor walls.

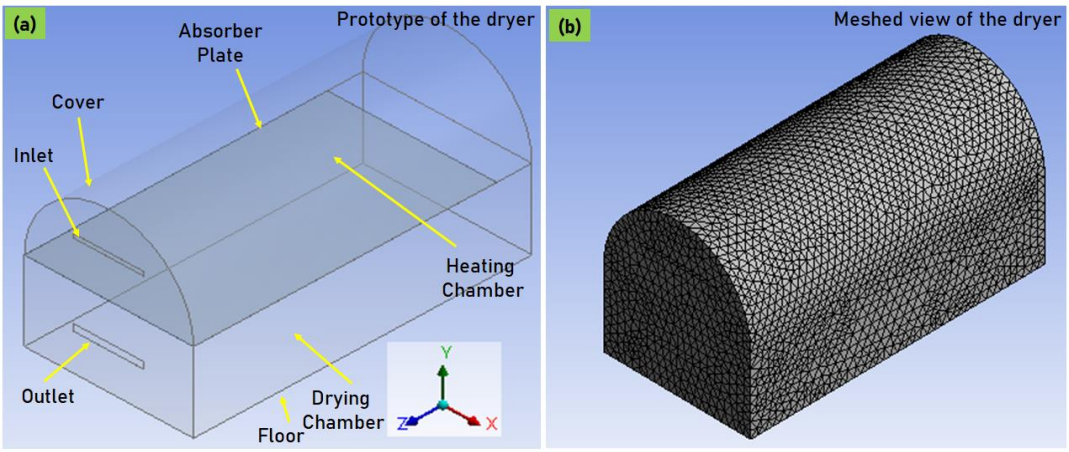

Fig. 1. The diagram of (a) the geometry and (b) meshing of the drying system

3. CFD Analysis

3.1. Turbulence Model

A forced convection flow field usually includes ventilation systems to drive the fluid throughout the chamber, which creates a turbulence movement due to the high flow rate and the heat transfer interaction in the flow field. This indicates that, the proposed drying system categories under turbulence flow. A mathematical model selected to predict the effects of turbulence inside the drying chamber was Realizable k–ε (epsilon) (the transport model of turbulent kinetic energy (κ) and its dissipation speed (ε)) with Non-equilibrium wall function, because of their high performance in more complex and main flow fields, accurately prediction of spreading rate, high convergence rate and comparatively low computational memory requirements.

3.2 Radiation Model

Solar radiation mainly depends on time, day, and month of the year, the mean solar time (GMT), geographical location, weather conditions, and STD or mesh orientation. The discrete ordinates (DO) model can solve the radiative transfer equation (RTE) for a finite number of discrete solid angles, each associated with a vector direction, and solve the irradiance at semi-transparent walls. Due to this, the discrete ordinates (DO) radiation model was used to simulate the effect of solar radiation inside the drying chamber. To simulate solar radiation; longitude of 36.8373^{o}, latitude of 7.6753^{o}, +3 GMT, and fear weather conditions were used. The orientation of the mesh is set as North on the negative X-direction and East on the positive Z-direction.

3.3 Species Transport

The species transport model is used to represent the mixture of two different types of fluid and to determine the mass fraction of each type inside the system. In this case, it is used to specify the mixture of dry air and water vapor. This simulation presents only the heat transfer model, where the mass transfer model is not included, because of this phenomenon there is no moisture transfer between the drying product and moist air. Due to this, the mass fraction of each species throughout the system is constant and there is no moisture diffusion on the solid walls. The mass fraction of moist air at the inlets of the drying chamber is 0.01. The executive summary of the operating conditions of the analysis is discussed in Table 1.

Table 1
The summary of operating conditions

Operating Conditions	Governing Equation
Solver	3D Simulation Implicit Formulation Pressure Based Absolute Velocity Formation Steady State Analysis
Gravity	9.81 m/s^2……Y-axis
Energy Equation	On
Viscose Model	Realizable $k-\varepsilon$ Model Non-equilibrium wall function
Radiation Model	Discrete Ordinate (DO)
Species Transport	On

3.4 Boundary Conditions

To obtain the desired result of the simulation, the boundary condition of the system must be defined carefully. The type of heat interaction between the boundaries with their appropriate values, the thickness of each boundary, and the type of material with their respective property must be defined. The drying system model contains inlet, outlet, absorber plate-wall, cover-wall, and floor-wall boundary conditions. The executive summary of boundary conditions of the analysis, the parameters used to define the condition with their value, and the type of material is discussed in Table 2.

Table 2
Summary of boundary conditions

Boundary conditions	Parameters	Values	Material
Inlet	Mass flow rate	0.0181 kg/s	Moist Air
	Temperature	300 K	
	Mass fraction	0.0101	
Outlet	Outlet pressure	0	Moist Air
	Mass Fraction	0	Moist air
Absorber plate-wall	Wall Thickness	0.0004 m	Black painted aluminum sheet
	Emissivity	0.95	
	Absorptivity	0.96	
	Heat transfer coefficient	3.076 W/m^{2}K	
Cover-wall	Wall thickness	0.0002 m	Semi-transparence polyethylene
	Emissivity	0.94	
	Absorptivity	0.02	
	Heat transfer coefficient	3.076 W/m^{2}K	
Floor-wall	Wall thickness	0.25 m	Bagasse
	Emissivity	0.88	
	Absorptivity	0.9	
	Heat transfer coefficient	3.023 W/m^{2}K	

3.5 Solution Methods

The solution method selected to perform the simulation is the Pressure-Velocity Coupling method for all models. Also, the spatial discretization methods used for the analysis of pressure are

second order, momentum, energy and water vapor is second order upwind and turbulent kinetic energy, turbulent dissipation rate, and discrete ordinate is first order upwind. the type of scheme, gradient, and initialization applied for each model is summarized in Table 3.

Table 3
The type of scheme, gradient, and initialization of each model

Type of scheme, gradient, and initialization	
Scheme	SIMPLEC
Gradient	Green-gauss node-based
Initialization	Hybrid

3.5.1 Energy and exergy

The rate of useful energy outcome is the difference of the final and initial thermal energy state of the air stream [32].

$$\dot{E}_U = \dot{m}_a C_{pa}(T_o - T_i) \tag{1}$$

Where, $\dot{E}_U$ is the useful energy (W), $\dot{m}_a$ is the mass flow rate of air (kg/s), C_{pa} is the specific heat of air (J/kg K), and T is the temperature (°C). The suffixes, 'o' is outlet and 'i' is inlet.

Thermal efficiency defined at the ratio of the useful thermal energy output and the incidence solar radiation over the projected area [33].

$$\eta_{th} = \frac{\dot{E}_U}{IA_{pr}} \tag{2}$$

Where, η_{th} is the thermal efficiency (%), $\dot{E}_U$ is the useful energy (W), I is the incidence solar radiation (W/m^2), and A_{pr} is the projected area (m^2).

The rate of exergy input is determined by [34].

$$\dot{E}_{xi} = IA_{pr}\left[1 - \left(\frac{4}{3} * \frac{T_{am}}{T_{sun}}\right) + \left(\frac{1}{3} * \left(\frac{T_{am}}{T_{sun}}\right)^4\right)\right] \tag{3}$$

Where, $\dot{E}_{xi}$ is the exergy inlet, T_{am} is the ambient temperature (K), and T_{sun} is the sun temperature (K).

The rate of exergy outcome is computed as [34].

$$\dot{E}_{xo} = \dot{m}_a C_{pa}\left[(T_o * T_{am}) + \left(T_{am} log\left(\frac{T_{am}}{T_{sun}}\right)\right)\right] \tag{4}$$

Where, $\dot{E}_{xo}$ is the exergy outlet, T_{am} is the ambient temperature (K), and T_{sun} is the sun temperature (K).

The exergy efficiency can be determined [35].

$$\eta_{ex} = \frac{\dot{E}_{xi}}{\dot{E}_{xo}} \tag{5}$$

Where, η_{ex} is the exergy efficiency.

4. Results and Discussion

This section illustrates the result obtained from the CFD simulation of a hemi cylindrical double air pass solar tunnel drying system with no load. The weather conditions data are essential for the analysis of the hourly variation of the temperature profile, the velocity and pressure distribution, and the exergetic performance of the newly designed solar tunnel drying system. Thus, the necessary ambient conditions are direct (beam) radiation, diffuse radiation, and ambient temperature were taken at a location ($7°40'0''\mathrm{N}, 36°50'0'\mathrm{E}$), and the hourly variation of ambient parameters on January 22, 2024 is presented in Figure 2(a) and the ambient temperature is shown in Figure 2(b). The higher direct radiation, diffuse radiation, and ambient temperature of the location were 1047 W/m^2, 61 W/m^2 and 28 ^{o}C at 7.00 A.M., respectively, as well as lower at forenoon and nightfall.

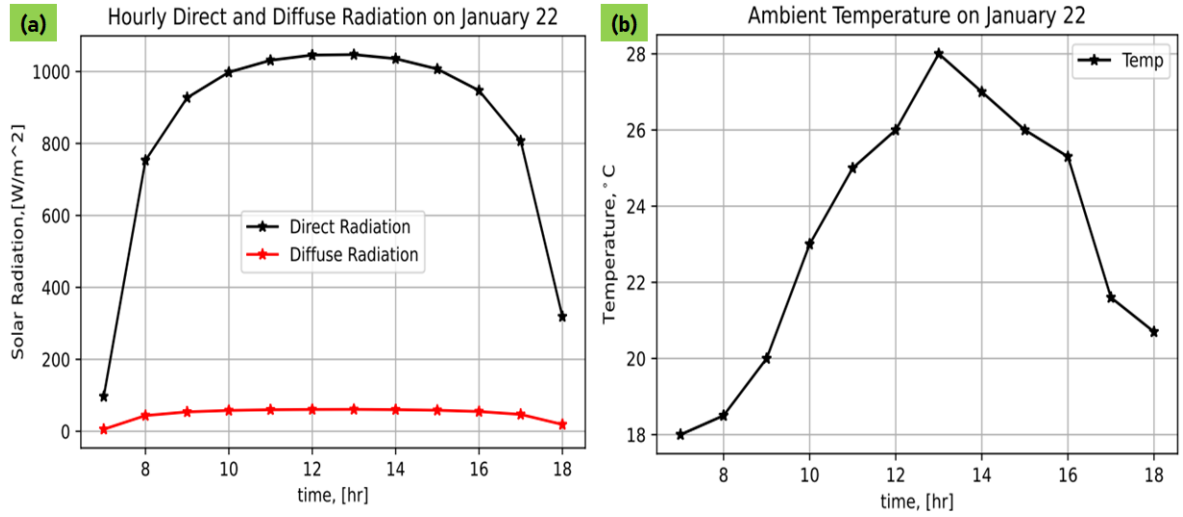

Fig. 2. The hourly variation of (a) direct and diffuse radiation and (b) ambient temperature on January 22, 2024

4.1 Hourly Variation of Temperature

The hourly average temperature at the outlet of the drying chamber was determined by performing a series of simulations for 12 sunshine hours of the day. Figure 3 is a graphical representation of the CFD simulation result of the outlet temperature of the drying chamber variation with time and demonstrates how the outlet temperature is affected by solar radiation and inlet temperature.

The result indicates that the maximum temperature encountered at the outlet of the drying chamber was 64.6 ^{o}C at 6.00 P.M. and 8.00 P.M. The value of temperature was above 50 ^{o}C for 10 hours and 60 ^{o}C for 6 hours of the day. This phenomenon confirmed that the evaporation rate of the drying system will be enhanced simultaneously drying period reduced and this will lead to the increment of daily drying capacity. The pattern of the temperature graph was similar to the graph of ambient conditions figure, where the maximum temperature value was found at noon and the lower value at sunrise and sunset due to the variation of solar radiation and inlet air temperature with time.

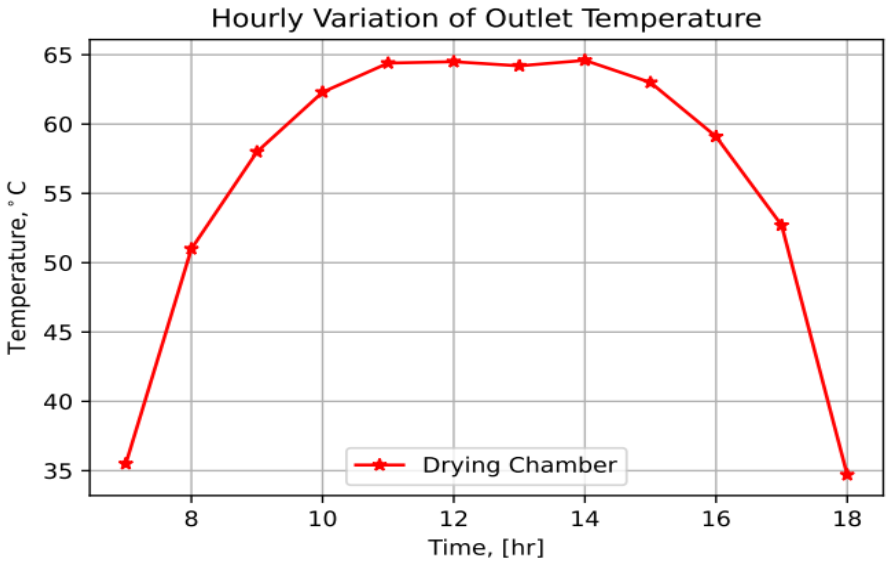

Fig. 3. Graph of hourly variation of temperature at the outlet drying chamber

Figure 4, is a pictorial presentation of the CFD result of the temperature distribution of air at the middle plane of both the heating and drying chamber for 12 hours and it illustrates the influence of solar radiation change over time on the temperature distribution. The highest value of the result is represented by red and the lowest value is by dark blue and also, green, yellow, and orange lie in the middle. Also, it contains 12 pictures of the temperature profile corresponding to 12 sunshine hours of the day starting from 7:00 am up to 6:00 pm. The result reveals that there is a uniform temperature distribution on the selected plane for all hours with a different value. In all pictures, the temperature on the right side is higher than on the left side due to the effect of the northern wall caused by the East-West orientation of the drying system and the location of ambient parameters used for the simulation which are found around the equator.

It also indicates that the higher temperature was observed at the center of the selected plane where the absorber plate is located and gradually decreases toward the cover wall inside the heating chamber for each hour. However, inside the drying chamber higher temperature was encountered on the south wall boundary and gradually decreased toward the north wall because of the effect of the northern wall. Also, a higher temperature was found on the internal surface of the floor and edgy wall boundaries due to insulation and its optimum thickness.

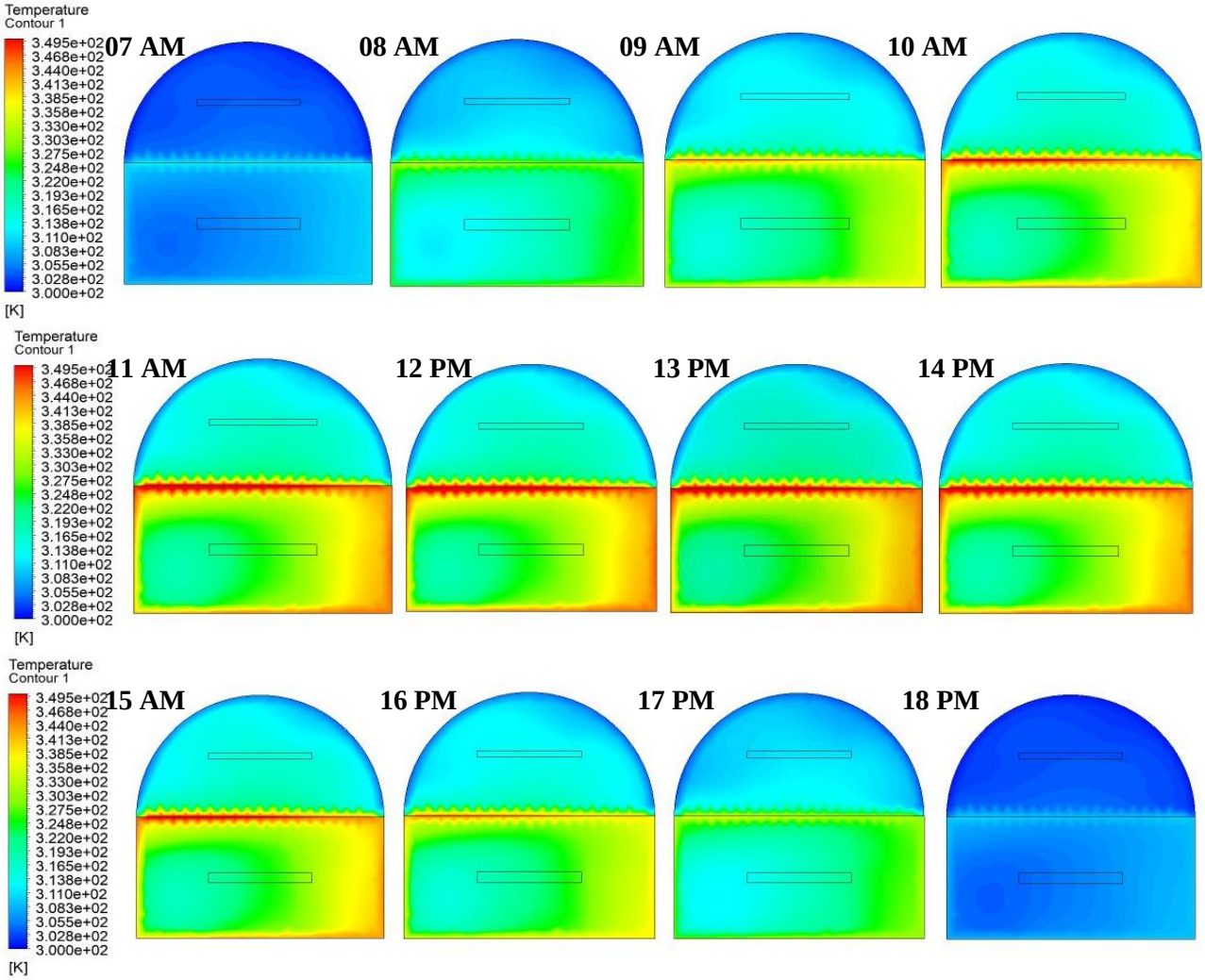

Fig. 4. Pictorial presentation of temperature distribution inside the heating and drying chamber for 12 hours

4.2 Temperature Distribution

The input parameters direct radiation, diffuse radiation, and a constant mass flow rate of 1047 W/m^2, 61 W/m^2, and 0.0181 kg/s, were used, respectively. Figure 5(a) presents the variation of temperature on the line drawn between the cover and the floor and demonstrates the temperature difference between the main components as well as the heating and drying chamber of the drying system (Figure 5(b)).

The highest temperature was observed on the absorber plate followed by the bottom floor, and the lowest value was found on the polyethylene cover. The material selected for the absorber plate was black-painted aluminum sheet metal with the ultimate solar radiation absorptivity coefficient and its direct exposure to the incidence of solar radiation which maximizes the thermal energy collecting capacity. This phenomenon makes the surface of the absorber plate maintain the highest temperature compared to the floor and cover boundaries. The temperature of the bottom floor and edge internal surface was higher than the cover surface due to their high absorptivity coefficient and the insulation material used has optimum thermos-physical properties and thickness. The material used for the cover has the highest solar radiation transmission ability up to 96% with a lower absorptivity coefficient also its outer surface is exposed to surroundings which enhances the thermal energy loss to the ambient and reduces the temperature.

It also demonstrates that throughout the drying system, a higher temperature was encountered inside the drying chamber than in the heating chamber, comparatively. The increment in the air stream temperature was observed in the drying chamber because it was reheated by the bottom surface of the absorber plate which enhances the thermal energy gain and the insulation material used reduces the thermal loss to the surroundings which leads to the enhancement of energy and exergy outcomes. However, the temperature at the outlet of the heating chamber is minimized because of heat loss to the ambient through the collector cover due to wind energy which increases the rate of convective heat transfer coefficient.

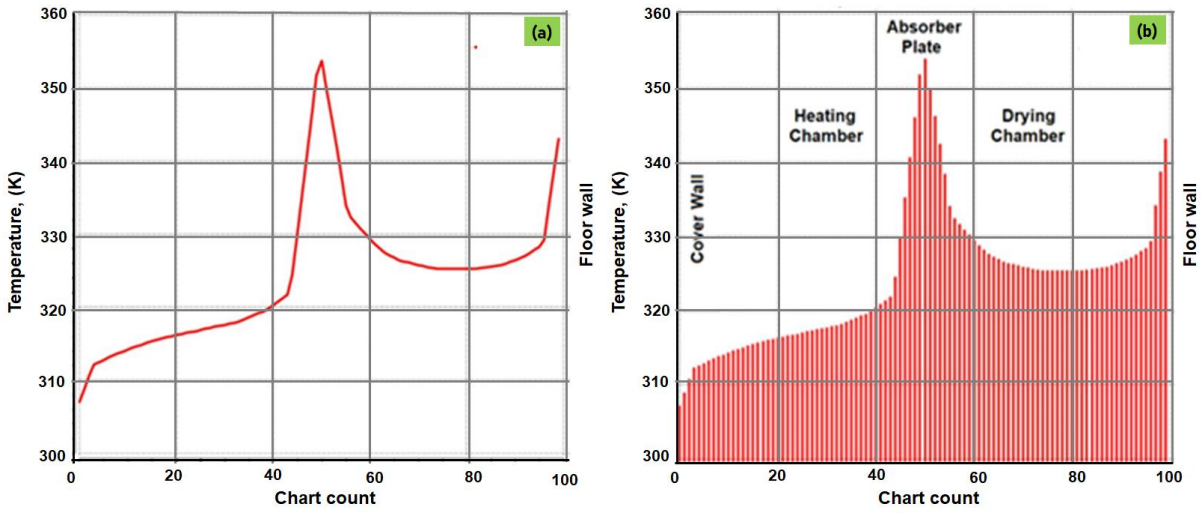

Fig. 5. (a) Temperature variation over the line drawn, and (b) temperature variation over heating chamber and drying chamber

Figure 6 shows the pictorial presentation of temperature distribution throughout the heating and drying chamber on January 22 at 7:00 pm. The temperature profile shows, that the uniformity of distribution inside the heating chamber was better compared to the drying chamber. Figure 6 shows the temperature distribution was almost uniform around the front and back walls of the drying chamber. This result is similar to the simulation result of Monish *et al.,* [36] and Yen *et al.,* [37].

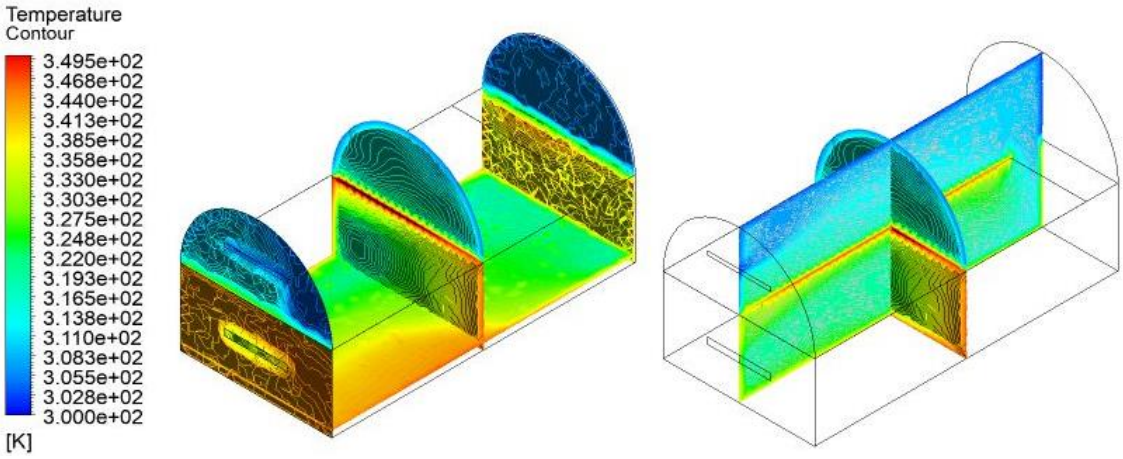

Fig. 6. Pictorial presentation of temperature distribution throughout the heating and drying chamber at 7:00 pm

Figure 7 presents the temperature variation over a line drawn between north-south, east-west, and top-bottom walls. The straight line used to plot graphs a, b, and c passes through the center of the drying system. Figure 7(a) shows that inside the heating chamber, the space between the plate and cover was higher at the center and lower around the edges due to this the temperature at the center is higher and lower around the edges because as the length of the space decreases the heat loss increases. However, inside the drying chamber, the value of temperature is higher around the edges and lower at the center due to insulation the temperature of the inner surface was higher.

Figure 7(b) shows that the temperature at the inlet of the heating chamber was lower and enhanced gradually by gaining thermal energy from the absorber plate up to the outlet and then flowing to the drying chamber. Also, the incoming air is reheated in the drying chamber and increases gradually from the inlet up to the outlet. Figure 7(c) indicates that in both chambers a higher temperature was observed around the absorber plate and continuously decreased toward the cover in the heating chamber and the floor in the drying chamber because a higher temperature was maintained by the plate comparatively.

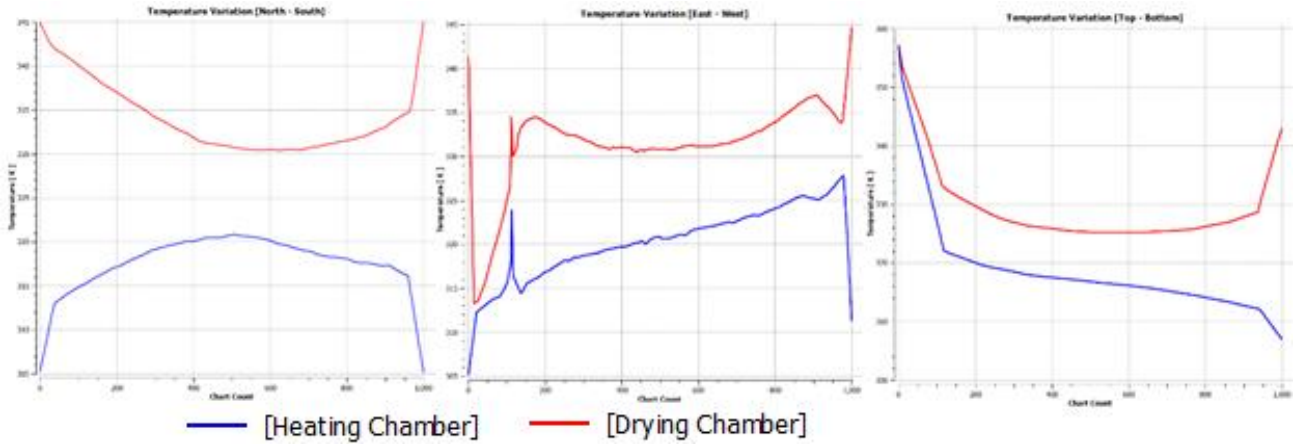

(a) (b) (c)

Fig. 7. The graph of temperature variation over the line drawn from (a) [North-South], (b) [East-West], and (c) [Top-Bottom] inside the heating and the drying chamber

4.3 Velocity Distribution

The velocity variation and distribution throughout the drying system were presented in Figure 8 by streamlines and in Figure 9 by velocity vectors. The result of the CFD simulation reveals that the maximum value of velocity is $1.123\ m/s$ at the outlet section, the minimum value is $0\ m/s$ around the solid wall boundaries and the average value of velocity throughout the drying chamber is $0.61\ m/s$. The result of average velocity was similar to the simulation result of Monish *et al.,* [31] and Yen *et al.,* [32], but the values are different, because of inlet mass flow rate, dimension, shape, size, number, and position of air inlet and outlet section difference.

The result of velocity streamline functions and velocity vector reveals that the higher turbulence observed around the inlet and outlet section of the heating and drying chamber, due to the higher velocity encountered and the cross-sectional area difference and also, the value of turbulence is lower in the other cross-section, due to velocity drop and pressure drop around the boundary surface of the solid domain (cover and floor inner wall). Pressure drop occurs due to the high viscosity of the air domain on the surface of solid boundaries.

Fig. 8. Velocity streamline of the drying system on January 22 at 7:00 am

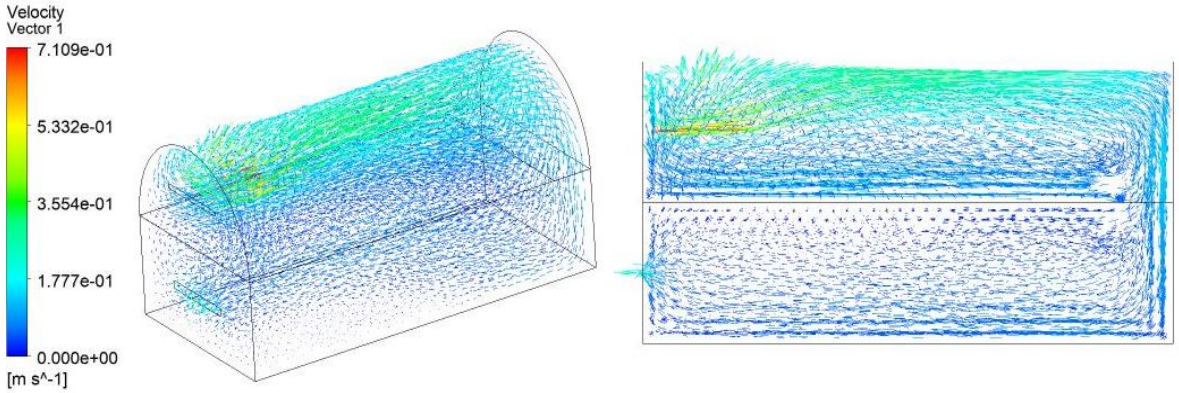

Fig. 9. Velocity vector of the drying system on January 22 at 7:00 am

4.4 Energy and Exergy

The hourly variation of useful energy outcomes and thermal efficiency of a double air pass solar tunnel drying system is presented in Figure 10(a). The result reveals that the maximum energy outcome was encountered before noon around 717.42 W/m^2. This is due to the increment of heat loss as the air stream temperature increases. The minimum value was observed at sunrise and sunset due to lower solar radiation input. Figure 10(b) shows that the maximum thermal efficiency was found at nightfall 34% where the thermal energy loss was lower. Whereas the lower value was observed at 7:00 pm. This is due to the increment of thermal energy loss as the solar radiation increases.

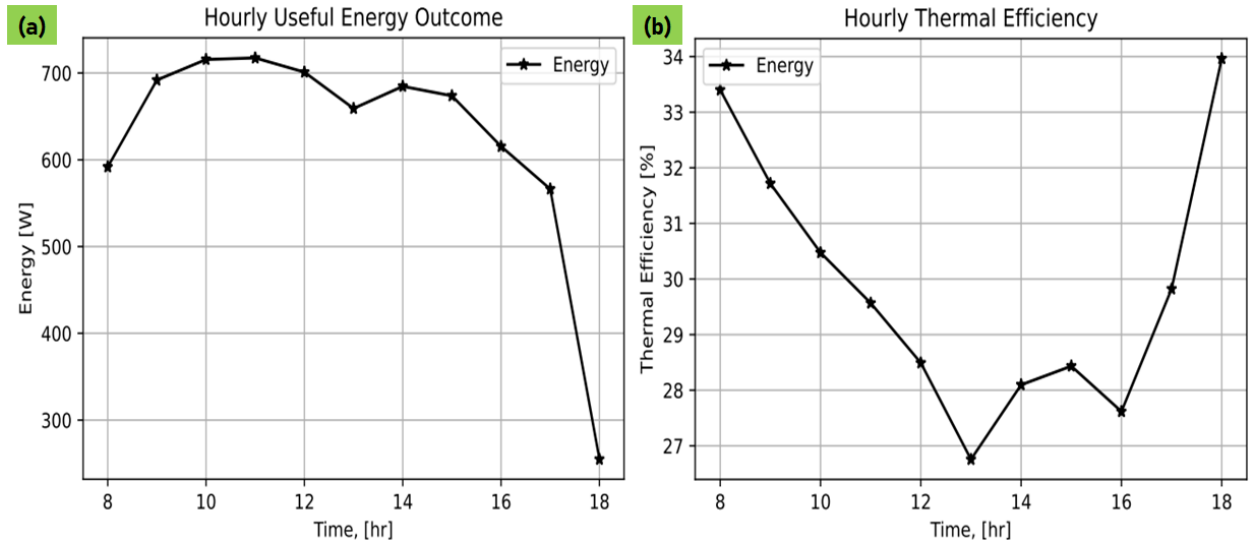

Fig. 10. The hourly variation of (a) useful energy outcomes and (b) thermal efficiency of the drying system

The hourly useful exergy outcome is provided in Figure 11(a) and the hourly exergy efficiency is given in Figure 11(b) along with the time. The average useful exergy outcome and exergy efficiency was found $166.7\ \mathrm{W/m^2}$ and 9.41%, respectively. The maximum useful work extraction was observed at 7:00 P.M. and the minimum value at sunset. Thus, the fluctuation of exergy performance with time was occurred by the variation of solar radiation and ambient temperature over time. In Table 4 comparison of present study results with the literature data is provided.

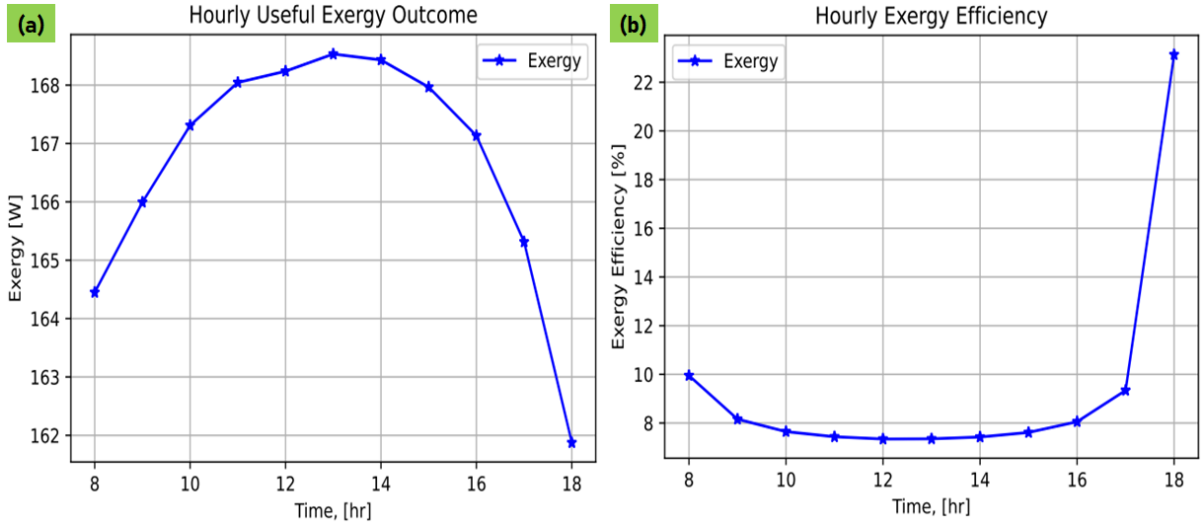

Fig. 11. The hourly variation of (a) useful exergy outcomes and (b) exergy efficiency of the drying system

Table 4
Comparison of present study with literature

Reference	Product type	Temperature	Thermal efficiency	Exergy efficiency
Sultan Karasu, and Ozdogan [3]	Thin-layer mushroom (agaricus bisporus)		59.74%, 67.66%, and 77.45% for natural convection dryer (NCD), forced convection dryer (FCD), and heat pump integrated dryer (HPD)	
Raja Sekhar *et al.,* [4]	Zingiber	33–74 °C	45%	--
Singh *et al.,* [5]	Fenugreek leaves (Trigonella foenum-graecum) and turmeric (Curcuma longa)		34.1%	--
Present study	Biomass briquettes	59.2^{o}C	30%	9.41%

4.5 Future Scope

The present study is limited to evaluate the energy and exergy analysis of single air pass solar tunnel dryer. Since the north wall insulation and entire drying time radiation toward the south wall may lessen heat loss from the dryer cabinet, the energy and exergy analysis may be evaluated with the insulation on the north wall. The analysis may extend to evaluate the heat transfer coefficients of drying material. The overall performance of the solar dryer at different weather conditions is also to be analysed in future. Different materials can be used for solar dryer for the evaluation of exergy and energy efficiency in future studies.

5. Conclusions

This work presents the CFD simulation of forced convection double air pass solar tunnel drying system was carried out to investigate the temperature and air distribution inside the heating and dryer chambers and to evaluate the thermal and exergy performance.

i. The simulation results revels that a higher temperature was maintained inside the drying chamber compared to the heating chamber.
ii. Flow parameters are uniformly distributed in both chamber due to a double air pass operating system.
iii. The energy and exergy performance of the newly developed drying system was enhanced due to the increment of air temperature and it increases the drying rate.
iv. The modified drying system will be applicable for agricultural and industrial drying process that requires high temperature.

Acknowledgement
Partial support from JiT Center of Excellence is gratefully acknowledged

References

[1] Ngusale, George K., Yonghao Luo, and Jeremiah K. Kiplagat. "Briquette making in Kenya: Nairobi and peri-urban areas." *Renewable and Sustainable Energy Reviews* 40 (2014): 749-759. https://doi.org/10.1016/j.rser.2014.07.206

[2] Guo, Zhenkun, Jianjun Wu, Yixin Zhang, Feng Wang, Yang Guo, Kening Chen, and Hu Liu. "Characteristics of biomass charcoal briquettes and pollutant emission reduction for sulfur and nitrogen during combustion." *Fuel* 272 (2020): 117632. https://doi.org/10.1016/j.fuel.2020.117632

[3] Asnaz, Melike Sultan Karasu, and Ayse Ozdogan Dolcek. "Comparative performance study of different types of solar dryers towards sustainable agriculture." *Energy Reports* 7 (2021): 6107-6118. https://doi.org/10.1016/j.egyr.2021.08.193

[4] Sekhar, Y. Raja, Adarsh K. Pandey, I. M. Mahbubul, Ghanta Ram Sai Avinash, Vaibhav Venkat, and Nitin Ralph Pochont. "Experimental study on drying kinetics for Zingiber Officinale using solar tunnel dryer with thermal energy storage." *Solar Energy* 229 (2021): 174-186. https://doi.org/10.1016/j.solener.2021.08.011

[5] Singh, Sukhmeet, R. S. Gill, V. S. Hans, and Manpreet Singh. "A novel active-mode indirect solar dryer for agricultural products: Experimental evaluation and economic feasibility." *Energy* 222 (2021): 119956. https://doi.org/10.1016/j.energy.2021.119956

[6] Kumar, Mahesh, Sunil Kumar Sansaniwal, and Pankaj Khatak. "Progress in solar dryers for drying various commodities." *Renewable and Sustainable Energy Reviews* 55 (2016): 346-360. https://doi.org/10.1016/j.rser.2015.10.158

[7] Mewa, Eunice A., Michael W. Okoth, Catherine N. Kunyanga, and Musa N. Rugiri. "Experimental evaluation of beef drying kinetics in a solar tunnel dryer." *Renewable energy* 139 (2019): 235-241. https://doi.org/10.1016/j.renene.2019.02.067

[8] Cetina-Quiñones, A. J., J. López López, L. Ricalde-Cab, Amina El Mekaoui, L. San-Pedro, and A. Bassam. "Experimental evaluation of an indirect type solar dryer for agricultural use in rural communities: Relative humidity comparative study under winter season in tropical climate with sensible heat storage material." *Solar Energy* 224 (2021): 58-75. https://doi.org/10.1016/j.solener.2021.05.040

[9] Mayor, L., R. Moreira, and A. M. Sereno. "Shrinkage, density, porosity and shape changes during dehydration of pumpkin (Cucurbita pepo L.) fruits." *Journal of food Engineering* 103, no. 1 (2011): 29-37. https://doi.org/10.1016/j.jfoodeng.2010.08.031

[10] Younsi, Ramdane, D. Kocaefe, S. Poncsak, Y. Kocaefe, and L. Gastonguay. "CFD modeling and experimental validation of heat and mass transfer in wood poles subjected to high temperatures: a conjugate approach." *Heat and Mass transfer* 44, no. 12 (2008): 1497-1509. https://doi.org/10.1007/s00231-008-0382-8

[11] Rao, Thota SS Bhaskara, and S. Murugan. "Solar drying of medicinal herbs: A review." *Solar Energy* 223 (2021): 415-436. https://doi.org/10.1016/j.solener.2021.05.065

[12] Leon, M. Augustus, S. Kumar, and S. C. Bhattacharya. "A comprehensive procedure for performance evaluation of solar food dryers." *Renewable and Sustainable Energy Reviews* 6, no. 4 (2002): 367-393. https://doi.org/10.1016/S1364-0321(02)00005-9

[13] Çakmak, Gülşah, and Cengiz Yıldız. "The drying kinetics of seeded grape in solar dryer with PCM-based solar integrated collector." *Food and bioproducts processing* 89, no. 2 (2011): 103-108. https://doi.org/10.1016/j.fbp.2010.04.001

[14] Baldán, Yanina, Anabel Fernandez, Andrés Reyes Urrutia, María Paula Fabani, Rosa Rodriguez, and Germán Mazza. "Non-isothermal drying of bio-wastes: Kinetic analysis and determination of effective moisture diffusivity." *Journal of environmental management* 262 (2020): 110348. https://doi.org/10.1016/j.jenvman.2020.110348

[15] Noh, Arina Mohd, Sohif Mat, and Mohd Hafidz Ruslan. "CFD simulation of temperature and air flow distribution inside industrial scale solar dryer." *Journal of Advanced Research in Fluid Mechanics and Thermal Sciences* 45, no. 1 (2018): 156-164.

[16] Sileshi, Senay Teshome, Abdulkadir Aman Hassen, and Kamil Dino Adem. "Simulation of mixed-mode solar dryer with vertical air distribution channel." *Heliyon* 8, no. 11 (2022). https://doi.org/10.1016/j.heliyon.2022.e11898

[17] Afshari, Faraz, Ataollah Khanlari, Azim Doğuş Tuncer, Adnan Sözen, İstemihan Şahinkesen, and Giovanni Di Nicola. "Dehumidification of sewage sludge using quonset solar tunnel dryer: an experimental and numerical approach." *Renewable Energy* 171 (2021): 784-798. https://doi.org/10.1016/j.renene.2021.02.158

[18] Al Smin, Ahmed Moh A., Alkbir Munir Faraj Almabrouk, Sairul Izwan Safie, Mohd Al Fatihhi Mohd Szali Januddi, Mohd Fahmi Hussin, and Abdulgader Alsharif. "Enhancing solar hybrid system efficiency in Libya through PSO & flower pollination optimization." *Progress in Energy and Environment* (2024): 23-31. https://doi.org/10.37934/progee.27.1.2331

[19] Karim, Abdul Razif Abdul, and Roslina Mohammad. "Meta-study of sensitivity analysis in solar renewable energy application." *Progress in Energy and Environment* (2023): 14-25. https://doi.org/10.37934/progee.23.1.1425

[20] Sulaiman, Nabila, Sany Izan Ihsan, Syed Noh Syed Abu Bakar, Zafri Azran Abdul Majid, and Zairul Azrul Zakaria. "Evacuated tubes solar air collectors: A review on design configurations, simulation works and applications." *Progress in Energy and Environment* (2023): 10-32. https://doi.org/10.37934/progee.25.1.1032
[21] Shameli, Kamyar, Siti Rahmah Aid, Nur Farhana Arissa Jonny, and Yutaka Asako. "Green Synthesis of Gold Nanoparticles Based on Plant Extract for Nanofluid-based Hybrid Photovoltaic System Application." *Journal of Research in Nanoscience and Nanotechnology* 4, no. 1 (2021): 19-34. https://doi.org/10.37934/jrnn.4.1.1934
[22] Nazer, Mohamed, Muhammad Fadzrul Hafidz Rostam, Se Yong Eh Noum, Mohammad Taghi Hajibeigy, Kamyar Shameli, and Ali Tahaei. "Performance analysis of photovoltaic passive heat storage system with microencapsulated paraffin wax for thermoelectric generation." *Journal of Research in Nanoscience and Nanotechnology* 1, no. 1 (2021): 75-90. https://doi.org/10.37934/jrnn.1.1.7590
[23] Zulakmal, Muhammad Yahya, Ahmad Fudholi, Nurul Shahirah Rukman, Nurul Syakirah Nazri, Chan Hoy Yen, Nilofar Asim, Sohif Mat, and Kamaruzzaman Sopian. "Computational fluid dynamics analysis of thermoelectric generators performance under solar photovoltaic-thermal (PVT) system." *Journal of Advanced Research in Fluid Mechanics and Thermal Sciences* 56, no. 2 (2019): 223-232.
[24] Ab Rashid, Nik Muhammad Hafiz Nik, Abdul Aziz Hairuddin, Khairil Anas Md Rezali, Siti Ujila Masuri, Jamiluddin Jaafar, and Deni Fajar Fitriyana. "Computational Fluid Dynamics (CFD) Validation and Investigation the Effect of Piston Bowl Geometries Performance on Port Fuel Injection-Homogeneous Charge Compression Ignition (PFI-HCCI) Engines." *Journal of Advanced Research in Numerical Heat Transfer* 18, no. 1 (2024): 30-48. https://doi.org/10.37934/arnht.18.1.3048
[25] Yanagita, Yoshiki, Kaishan Feng, Yuko Miyamura, Adi Azriff Basri, Mohammad Zuber, Siti Rohani, Abdul Aziz, Kamarul Arifin Ahmad, and Masaaki Tamagawa. "Evaluation of Virus Concentration Analysis in the Airway by CFD." *Journal of Advanced Research in Numerical Heat Transfer* 13, no. 1 (2023): 96-105. https://doi.org/10.37934/arnht.13.1.96105
[26] Jahan, Sultana, M. Ferdows, M. D. Shamshuddin, and Khairy Zaimi. "Effects of solar radiation and viscous dissipation on mixed convective non-isothermal hybrid nanofluid over moving thin needle." *Journal of Advanced Research in Micro and Nano Engineering* 3, no. 1 (2021): 1-11.
[27] Alawi, Omer A., and Haslinda Mohamed Kamar. "Performance of Solar Thermal Collector Using Multi-Walled Carbon Nanotubes: Simulation Study." *Journal of Advanced Research in Micro and Nano Engineering* 2, no. 1 (2020): 12-21.
[28] Khairi, Ahmad Adzlan Fadzli, Abdullah Yassin, Abang Mohammad Nizam Abang Kamaruddin, Mohamed Sukri Mat Ali, and Nurshafinaz Maruai. "Numerical Simulation of Drying Process within a Novel Rotary Drying Machine for Palm Oil Sludge." *Journal of Advanced Research in Applied Mechanics* 103, no. 1 (2023): 33-42. https://doi.org/10.37934/aram.103.1.3342
[29] Ismail, Iman Fitri, Akmal Nizam Mohammed, Bambang Basuno, Siti Aisyah Alimuddin, and Mustafa Alas. "Evaluation of CFD Computing Performance on Multi-Core Processors for Flow Simulations." *Journal of Advanced Research in Applied Sciences and Engineering Technology* 28, no. 1 (2022): 67-80. https://doi.org/10.37934/araset.28.1.6780
[30] Akter, Farzana, Kazi Ahasan Ekram, Md Araful Hoque, and Mohammad Joynal Abedin. "An Assessment of Solar Micro-Grid System in the Islands of Bangladesh for Sustainable Energy Access." *Malaysian Journal on Composites Science and Manufacturing* 12, no. 1 (2023): 31-42. https://doi.org/10.37934/mjcsm.12.1.3142
[31] Koli, Chandra Shekhar, M. K. Gaur, and Pushpendra Singh. "Energy and exergy assessment of a novel parabolic hybrid active greenhouse solar dryer." *Solar Energy* 245 (2022): 211-223. https://doi.org/10.1016/j.solener.2022.09.021
[32] Ucar, A., and M. Inallı. "Thermal and exergy analysis of solar air collectors with passive augmentation techniques." *International communications in heat and mass transfer* 33, no. 10 (2006): 1281-1290. https://doi.org/10.1016/j.icheatmasstransfer.2006.08.006
[33] Esen, Hikmet. "Experimental energy and exergy analysis of a double-flow solar air heater having different obstacles on absorber plates." *Building and Environment* 43, no. 6 (2008): 1046-1054. https://doi.org/10.1016/j.buildenv.2007.02.016
[34] Bejan, Adrian. *Entropy generation minimization: the method of thermodynamic optimization of finite-size systems and finite-time processes*. CRC press, 2013..
[35] S. Chamoli, Exergy analysis of a flat plate solar collector, *J. Energy Southern Afr*. 24 (3) (2013) 8–13.
[36] Monish. M, Ramnath. S, Manojkumar. S, Jeeva S., "Solar Tunnel Air Dryer: A Computational Fluid Dynamics Investigation For The Flow Path Design With The Temperature Distribution". *Int. J. Mechanical and Production* 7(8) (2018): 263-273.
[37] Duong, Yen HP, Nhan T. Vo, Phung TK Le, and Viet T. Tran. "Three-Dimensional Simulation of Solar Greenhouse Dryer." *CET Journal-Chemical Engineering Transactions* 83 (2021). https://doi.org/10.3303/CET2183036